Cyclic tests on hybrid inter-module joints with high-damping rubber

Konstantinos Daniel Tsavdaridis[1][0000-0001-8349-3979] and Dan-Adrian Corfar[1][0000-0002-9843-2973]

[1] City, University of London, London, UK
Konstantinos.Tsavdaridis@city.ac.uk

Abstract. Recently, a novel hybrid inter-module connection was proposed to reduce the permanent damage in the volumetric module by employing a rubber bearing. In this study, two cyclic tests were carried out to study the seismic performance of the hybrid inter-module connection at joint level, while also determining the effect of the beam-column connection detail. The standard FEMA/SAC loading sequence was employed on single-span, meso-scale joint prototypes with bi-axial loading applied to the top post. The results showed that the hybrid IMJs exhibited nonlinear, multi-stage hysteretic responses, governed by the bending resistance of the bolting assembly and the stiffness of the intra-module connection. In terms of the aseismic performance, the joints exhibited remarkably low residual drifts, below the repairability limit of 0.5% up to 2% drift ratio, while displaying relatively high equivalent viscous damping coefficients during the first stages of deformation owing to the effectives of the high-damping rubber bearing. Overall, the cyclic tests demonstrated the feasibility of the proposed connection, which delayed the contribution of the members in the lateral response of the joints, limiting the damage suffered by the volumetric module in the aftermath of an earthquake.

Keywords: Steel Modular Buildings, Inter-module Joints, Hybrid Connections, Intra-module Connections, High-Damping Rubber, Cyclic Load.

1 Introduction

Steel modular building systems (MBSs) have risen in popularity due to the widely recognised advantages of modular construction [1], while the excellent strength-to-weight ratio of structural steel has enabled the advancement of the technology to new heights [2]. As previous research has showed, inter-module connections (IMCs) play a crucial role in the lateral behaviour of self-standing steel modular buildings [3–6]. Thus far, a lot of effort has been put into the development of full-strength/rigid inter-module joints (IMJs) which demonstrate good seismic performance based on capacity design which ensures that the seismic-input energy is dissipated through the hysteresis of the steel beams [7–10]. However, the significant

permanent damage developed in the volumetric module hinders its demountability and reusability, while the large residual deformations greatly affect the functionality and repairability of a steel modular building in the aftermath of an earthquake. Therefore, the subject of earthquake-resilient steel modular buildings with energy-dissipating and/or self-centring components integrated within the inter-module joints has captured the interest of researchers [11–14]. In this regard, the authors have recently proposed a hybrid IMC employing a high-damping rubber bearing and a bolting assembly and investigated its cyclic behaviour at connection level through validated proof-of-concept finite element analysis (FEA) [15]. In this study, two cyclic tests were carried out to study the seismic performance of the hybrid IMC at joint level, while also determining the effect of the beam-column (intra-module) connection.

2 The proposed hybrid inter-module connection

A schematic of the proposed connection was shown in Fig. 1a. The connection has been designed to fulfil the essential functions of vertical and horizontal connectivity between modules, while the centred alignment of the member cross-sections to the box corners eliminates the unfavourable effect of eccentric loads caused by offsets. Axial compression is transferred between the corner posts through the laminated elastomeric bearing made with steel reinforcing plates to control the level of vertical displacement, whereas tensile axial force would be resisted by the bolting assembly. Horizontal shear forces are transferred through a combined mechanism of friction between the faying steel surfaces, shear resistance of the rubber bearing, and bending of the bolt rod, while the interlocking pins prevent accidental sliding. To improve the energy dissipation capacity of the rubber bearing at the shear deformation levels expected in the IMC (50%-100% shear strains), the rubber layers were made of high-damping (filled) rubber instead of low-damping (unfilled) rubber, as the addition of carbon black filler improves the hysteresis of rubber [16,17].

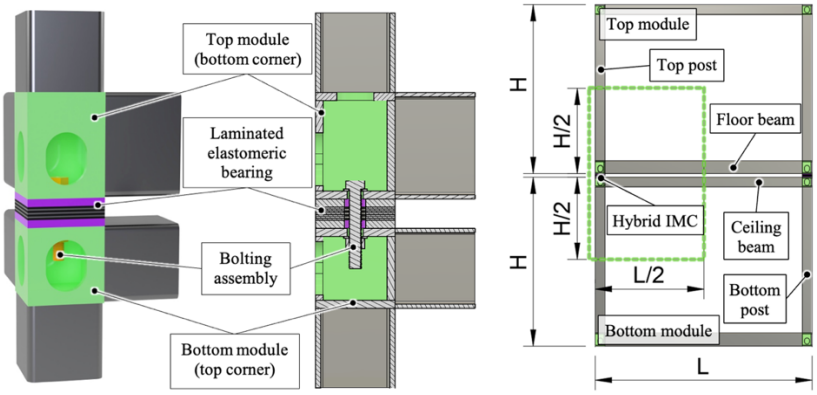

a. Configuration details b. Meso-scale joint prototype

Fig. 1. Hybrid inter-module connection.

3 Experimental programme

3.1 Details of the test specimens

The test IMJ prototypes were made of top and bottom beam-column subassemblages, and the inter-module connection between them. The meso-scale configuration (Fig. 1b) was adopted as a cost-effective solution that replicates the deformed shape and anticipated points of inflection in planar modular frames subjected to in-plane lateral loads by limiting the lengths of the posts and beams to half of those in the full-size frame panel.

Table 1. Test specimens.

Joint prototype	Bolting assembly	Beam-column joint
JP01	M24, class 8.8 bolt	Unstiffened
JP02	M24, class 8.8 bolt	Stiffened

As summarised in Table 1, two specimens namely JP01 and JP02 were designed to investigate the influence of the intra-module connection's stiffness on the seismic performance of the hybrid IMJs at joint level by considering two details of beam-column joints (stiffened and unstiffened).

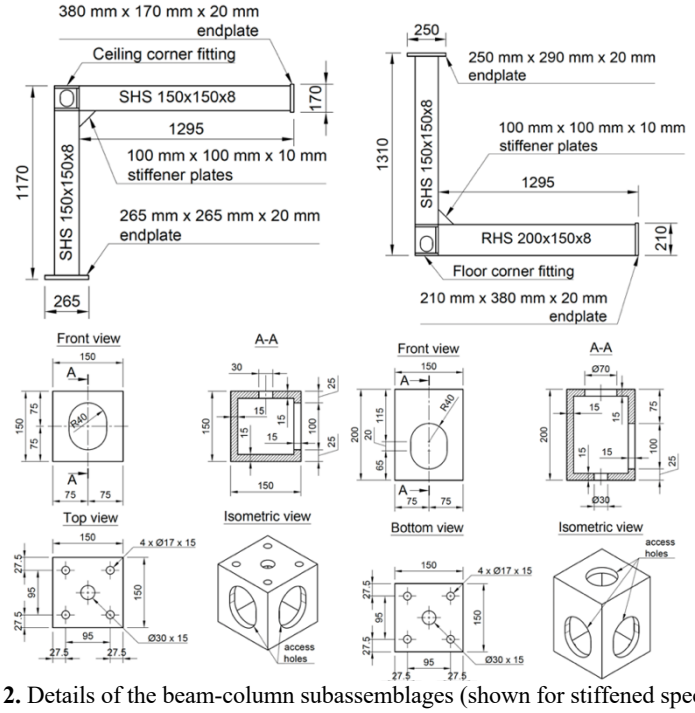

Fig. 2. Details of the beam-column subassemblages (shown for stiffened specimen).

The top and bottom beam-column subassemblages (Fig. 2) were S355J2H steel cold-formed hollow members, joined to S355J2H steel-plated box corner fittings by complete joint penetration (CJP) groove welds. The box corner fittings were fabricated from 15-mm-thick steel plates. Two S355J2H steel stiffeners of 100 mm x 100 mm x 10 mm triangular plate were welded at the beam-column connection for the stiffened specimen.

The rubber bearings (Fig. 3) were made of two outer S355 steel plates (150 mm x 150 mm x 15 mm), four high-damping rubber layers (150 mm x 150 mm x 4 mm) and three steel shims (150 mm x 150 mm x 3 mm), designed to achieve a shape factor of S = 8.85 to improve the stability of the bearing and limit the bulging of the rubber layers under the applied axial load.

Each bolting assemblies consisted of standard M24 x 150mm full-thread hexagon head bolts for specimens JS-1 and JS-2 and an M27 x made of class 8.8 high-strength steel (HSS).

The main properties obtained from material characterisation tests were summarised in Table 2 for the S355 steel and Table 3 for the high-damping rubber compound.

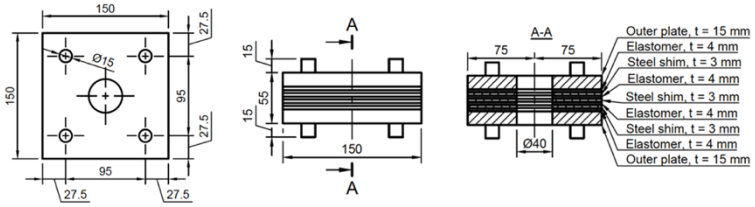

Fig. 3. Geometry of the rubber bearings.

Table 2. Material properties of the steel frame members.

Part	Steel grade	E[a] (GPa)	f_y[b] (N/mm^2)	f_u[c] (N/mm^2)	A[d] (%)
Top post	S355J2H	209	505	546	28.2
Bottom post	S355J2H	205	438	496	30.9
Floor beam	S355J2H	190	433	507	32.4
Ceiling beam	S355J2H	202	541	565	19.5

[a] Modulus of elasticity, [b] Yield strength, [c] Tensile strength, [d] Elongation percentage

Table 3. Material properties of high-damping rubber.

Hardness [a]	Shear modulus, G [c]	Effective damping ratio, $\xi_{eff,b}$[c]
86 IRHD[b]	0.61 MPa	18.46 %

[a] based on shear modulus at 5% shear strain, [b] International rubber hardness degree, [c] at 100% shear strain

3.2 Test setup

The test setup was depicted in Fig. 4. The loading system was designed to accommodate the bi-axial loading applied to the top column of the IMJ prototypes, while realistically replicating the deformed shape of unbraced modular frames subjected to a lateral load as recommended by Lacey et al. [18]. The joint prototypes were assembled directly within the self-reacting test frame in a straightforward sequence by stacking the lower sub-assemblage, the rubber bearing, and the upper sub-assemblage, followed by the insertion of the bolting assemblies. A snug-tight condition was achieved by the full effort of manually tightening the bolts with a spanner through the corner fitting access holes.

The test followed the prequalification and cyclic qualification testing provisions as per ANSI/AISC 341-22 [19], applying the displacement-controlled standard FEMA/SAC [20] loading sequence shown in Fig. 4, through the horizontal actuators in a quasi-static manner at a rate of 10mm/min to limit the influence of dynamic effects such as those arising from the inertial forces of the joint prototype members. To capture the effect of gravitational loading, an axial load equivalent to 5% of the compressive yield capacity, $N_{c.Rd}$, (using nominal material properties as per Eurocode 3, Part 1 [21]) was kept constant throughout the test. The vertical load exerted a compressive stress of 4.7 MPa on the rubber bearing.

Due to the deflection of the rubber layers under the applied axial load, the bolting assemblies experienced a partial loss of pre-tension, losing the preliminary snug-tight condition. While this effect led to slightly lower shear stiffness in the connections during the early cycles, it allowed for a larger deformation capacity and provided a strength reserve by effectively delaying the full contribution of the studs and bolts to the force-transfer mechanism of the connections.

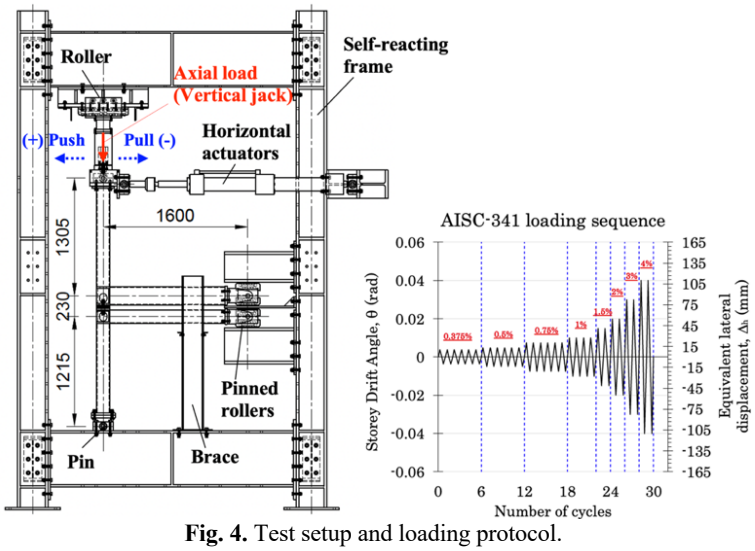

Fig. 4. Test setup and loading protocol.

4 Results and discussion

4.1 Test phenomena and controlling failure modes

At the onset of cyclic loading, the inter-storey drift occurred mostly in the inter-module connection, as expected due to the low shear stiffness of the rubber layers, highlighting the rubber bearing as the major contributor to the joint's response to small-amplitude lateral loads. During these initial stages, it was observed that the bolting assemblies were allowed to translate horizontally together with the upper box corner fittings until the gap provided by the bolt hole tolerance was fully closed and the bolting assemblies became locked in a bending deformation state. Then, as the loading sequence progressed towards the larger drift ratio levels, the shear deformation of the rubber layers increased up to the point when the contribution of the flexural stiffness of the beam-column sub-assemblages was evident as shown in Fig. 5 by the pronounced deflection of their framing members.

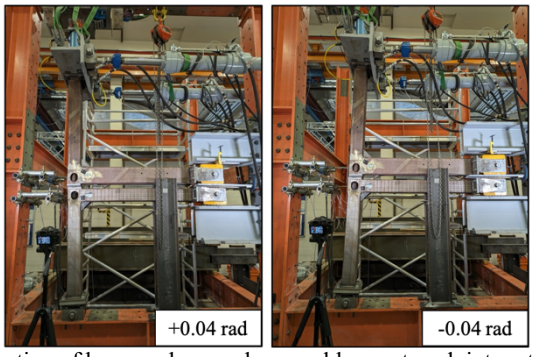

Fig. 5. Deflection of beam-column sub-assemblages at peak inter-storey drift ratio.

Taking a closer look at the connection level, the rubber bearing was subjected to the combined effect of axial load and horizontal shear throughout the cyclic loading protocol. Due to the quasi-static nature of the tests and the low thickness of the rubber layers, heat build-up was not expected to be an issue, which was confirmed with the aid of a thermal camera, registering a constant temperature throughout the test. There was no gap opening between the box corner fitting end-plates and the outer plates of the rubber bearing, as the top and bottom surfaces remained parallel even at maximum shear deformation levels, as shown in Fig. 6.

During the test on specimen JP01, the M24 HSS bolt experienced significant bending deformation as well as damage to the threads (Fig. 7). The onset of weld cracking at the ceiling beam-column connection (Fig. 8a) was noticed after the peak was reached in the positive loading direction during the second ±4% drift ratio cycle, causing the peak lateral load in the reverse direction to fall to 85% of the previous maximum.

At the end of the load programme, the reduction was still well above the 20% failure criterium defined in the FEMA/SAC guidance [20], yet the controlling

failure mode could be identified as the weakened beam-column connection. This finding was in good agreement with results from similar tests [22–24], emphasising once more the importance of the weld quality at these highly stressed regions.

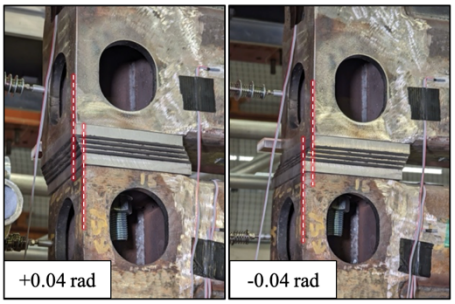

Fig. 6. Shear deformation of the rubber layers.

Specimen JP02 suffered similar damage levels to the HSS bolt (Fig. 7), while the test was completed without noticeable damage to the beam-column connection (Fig. 8b) and framing members due to the effect of the stiffener plates.

Even though no fracture occurred in the threads, the significant deformation in the shanks of the HSS bolts may lead to the assumption that the bolts failed, and therefore the ultimate limit state design of the hybrid joint would be controlled by the bending resistance of the bolting assembly. Moreover, the results proved that it is desirable to add stiffeners at the intra-module connections, to ensure that the controlling failure mode is indeed governed by the bending of the bolt rod and by the resistance of the weld at the beam-column joint.

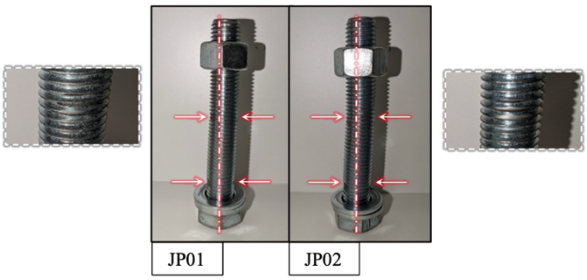

Fig. 7. Bolt deformation and damage to threads.

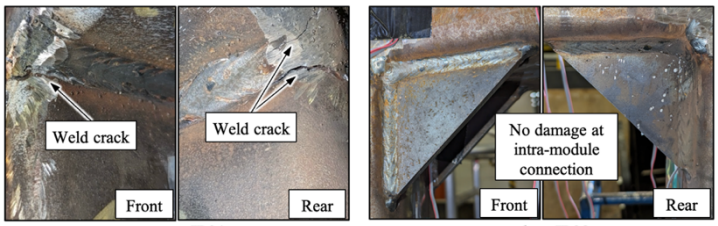

a. JP01 b. JP02

Fig. 8. State of the intra-module connection in bottom module at the end of the test.

4.2 Hysteresis loops

The relationship between the applied lateral displacement and the corresponding reaction force at the top of the IMJ prototypes was shown in Fig. 9.

Both specimens displayed similar reverse S-shaped curves with well-defined, stable hysteresis and multiple stages indicating the successive activation of different connection components.

During the first stage (0 to ±0.5% drift ratio), the rubber bearing was immediately engaged by the horizontal shear developed between the box corner fittings of the IMC due to the frictional resistance of the steel contact surfaces.

In the second stage (±0.5% to ±3%), the bolting assembly was completely engaged in a bending deformation as the bolt hole clearances closed under the relative horizontal displacement of the box corner fittings. This limited the shear deformation in the rubber layers, initiating the partial involvement of the framing members through their flexural stiffness.

The third and final stage (±3% and beyond) was identified by the comparison between the stiffened and unstiffened beam-column connections, signalling the prominent influence of the intra-module connection in the force resisting mechanism developed at high drift ratios.

Overall, the IMJs displayed stiffer behaviour in the negative loading direction (pulling direction for the actuators), which was attributed to the lack of symmetry of the one-sided T-shaped specimens, with rigid intra-module beam-column connections only on one side of the assemblage. This finding was in good agreement with the results from other experimental work that employed one-sided T-shaped joints with column loading [22,24].

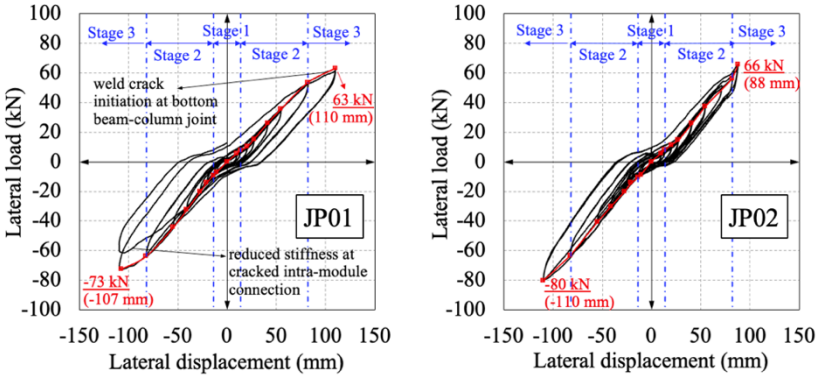

Fig. 9. Hysteresis loops.

4.3 Residual drift

The residual deformation of the two specimens at each inter-storey drift level was shown in Fig. 10, represented the percent ratio of the residual displacement corresponding to zero lateral load during load reversal and the total specimen height.

Comparing the results to the residual drift limits defined by FEMA P-58-1 [25], the specimens exhibited similar results up to 1% drift ratio, with residual drifts below the realignment limit of 0.2% in the negative loading direction, while the residual deformation was generally below or slightly fluctuating near the 0.5% repairability limit until the 2% drift ratio was reached and still economically feasible to repair up to 3% drift level. Above the 1% residual drift limit, the major realignment required to restore the safety of the building may render the structure as unfeasible to repair. At 4% drift ratio, the residual drift of the unstiffened specimen was larger by 0.2% than that of the stiffened joint in the negative loading direction, emphasising the favourable influence of the intra-module connection on the re-centring ability when designed to perform elastically.

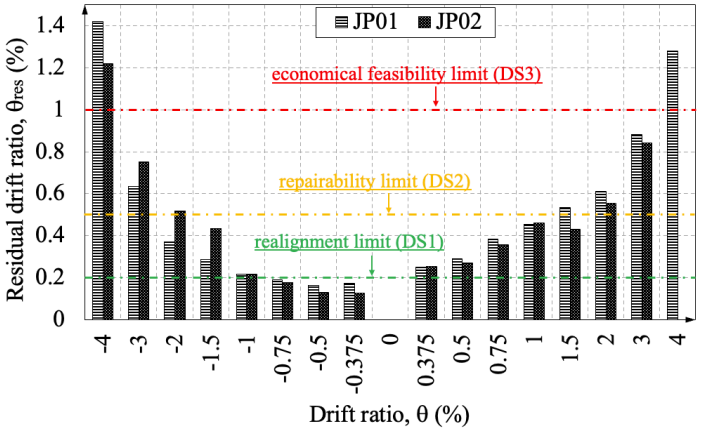

Fig. 10. Residual deformation levels in the hybrid IMJs.

4.4 Energy dissipation capacity

Fig. 11a shows the total energy dissipated in the first cycle, E_D, at each drift ratio level, represented by the area enclosed by the hysteresis loops. The reduced values up to 2% drift ratio confirmed the limited inelastic deformation of the frame members which performed elastically, while the sudden spike in the energy dissipated during the 3%-4% drift ratios was mostly attributed to frame members hysteresis, confirming their late activation during the third stage.

Fig. 11b illustrated the variation of the equivalent viscous damping coefficients, ξ_{eq}, at different drift ratios, showing significantly higher equivalent viscous damping coefficients during the early stages, followed by a progressive decrease and a slight recovery after the 2% drift ratio level. This finding was quite unique when compared to the variation of the equivalent viscous damping, provided by steel yielding mechanisms, which usually starts close to zero followed by a steady increase with the progression of the cyclic loading. The remarkable behaviour of the hybrid joints was attributed to the activation of the rubber bearings during the early stages of loading and to the mechanical properties of the high-damping rubber

compound used in the rubber layers, while the recovery after the 2% drift ratio was correlated with the engagement of the steel frame elements during the third stage of deformation observed on the hysteresis loops. The detail of the intra-module connection did not have a significant influence on the energy dissipation capacity of the joint up to the deformation levels achieved in the tests, while the differences observed at 4% drift ratio resulted from the reduced displacement reached by the actuators during the test on JP02 due to a malfunction of the control system.

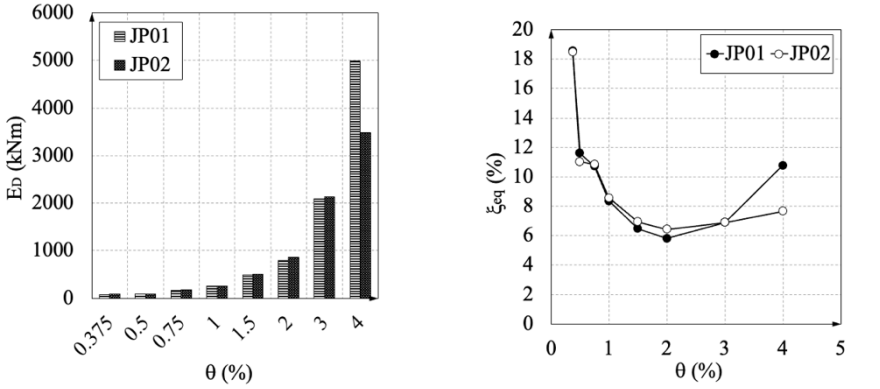

a. Energy dissipation b. Equivalent viscous damping coefficient

Fig. 11. Energy dissipation capacity of the IMJs.

5 Conclusions

In this study, two inter-module joint (IMJ) prototypes equipped with a novel hybrid inter-module connection were tested under cyclic loading to evaluate their aseismic performance and determine the effect of the intra-module connection detail.

The hybrid IMJs exhibited nonlinear hysteretic responses characterised by the sequential activation of different connection components at three different stages. The first stage was governed by the low shear stiffness of the rubber bearing, the second stage reflected the key influence of the bolting assembly, now fully engaged by the shear deformation in the rubber bearing, while the third stage highlighted the role of the intra-module connection stiffness.

The intra-module connections should be designed to perform elastically by adding stiffeners to the beam-column joint in order to ensure that the controlling failure mode of the joints is governed by the bending of the HSS bolts.

Both specimens exhibited remarkably low residual drifts, below the repairability limit of 0.5% up to 2% drift ratio, while the higher equivalent viscous damping coefficients registered during the first stages of deformation emphasised the effectiveness of the high-damping rubber compound.

Overall, the cyclic tests demonstrated the feasibility of the proposed connection, which effectively delayed the full participation of the members in the lateral

response of the joints, limiting the damage suffered by the volumetric module in the aftermath of an earthquake. Now, design recommendations should be developed to allow the necessary deformation capacity in the bolt rod at the required lateral load capacity of the hybrid joint, while further effort should be put into maximising the energy dissipation capacity of the hybrid IMC without affecting its re-centring capabilities or increasing the permanent damage in the volumetrics.

References

1. Ferdous W, Manalo A, Sharda A, Bai Y, Ngo TD, Mendis P (2022) Construction Industry Transformation Through Modular Methods. In: Ghaffar SH, Mullett P, Pei E, Roberts J, editors. Innovation in Construction, Cham: Springer, p. 259–76. https://doi.org/10.1007/978-3-030-95798-8_11.
2. Thai H-T, Ngo T, Uy B (2020) A review on modular construction for high-rise buildings. Structures 28:1265–90. https://doi.org/10.1016/j.istruc.2020.09.070.
3. Corfar D-A, Tsavdaridis KD (2022) A comprehensive review and classification of inter-module connections for hot-rolled steel modular building systems. Journal of Building Engineering 50:104006. https://doi.org/10.1016/j.jobe.2022.104006.
4. Farajian M, Sharafi P, Eslamnia H, Kildashti K, Bai Y (2022) Classification of inter-modular connections for stiffness and strength in sway corner-supported steel modular frames. Journal of Constructional Steel Research 197:107458 https://doi.org/10.1016/j.jcsr.2022.107458.
5. Wang Z, Tsavdaridis KD (2022) Optimality criteria-based minimum-weight design method for modular building systems subjected to generalised stiffness constraints: A comparative study. Engineering Structures 251:113472. https://doi.org/10.1016/j.engstruct.2021.113472.
6. Wang Z, Rajana K, Corfar D-A, Tsavdaridis KD (2023) Automated minimum-weight sizing design framework for tall self-standing modular buildings subjected to multiple performance constraints under static and dynamic wind loads. Engineering Structures 286:116121. https://doi.org/10.1016/j.engstruct.2023.116121.
7. Dai X-M, Zong L, Ding Y, Li Z-X (2019) Experimental study on seismic behavior of a novel plug-in self-lock joint for modular steel construction. Engineering Structures 181:143–64. https://doi.org/10.1016/j.engstruct.2018.11.075.
8. Chen Z, Wang J, Liu J, Khan K (2021) Seismic behavior and moment transfer capacity of an innovative self-locking inter-module connection for modular steel building. Engineering Structures 245:112978. https://doi.org/10.1016/j.engstruct.2021.112978.
9. Zhai S-Y, Lyu Y-F, Cao K, Li G-Q, Wang W-Y, Chen C (2023) Seismic behavior of an innovative bolted connection with dual-slot hole for modular steel buildings. Engineering Structures 279:115619. https://doi.org/10.1016/j.engstruct.2023.115619.
10. Yang C, Chen H, Wen H, Wang Q, Zhang B, Ou J (2024) Experimental study on seismic performance of internal cruciform joints of grouting sleeve connection for modular integrated construction. Engineering Structures 301:117325. https://doi.org/10.1016/j.engstruct.2023.117325.
11. Sultana P, Youssef MA (2016) Seismic performance of steel moment resisting frames utilizing superelastic shape memory alloys. Journal of Constructional Steel Research 125:239–51. https://doi.org/10.1016/j.jcsr.2016.06.019.

12. Sendanayake SV, Thambiratnam DP, Perera NJ, Chan THT, Aghdamy S (2021) Enhancing the lateral performance of modular buildings through innovative inter-modular connections. Structures 29:167–84. https://doi.org/10.1016/j.istruc.2020.10.047.
13. Zhang G, Xu L, Li Z (2023) Development and Experimental Verification of Self-Centering Haunched Plug-In Modular Connections. J Struct Eng 149:04023047. https://doi.org/10.1061/JSENDH.STENG-12029.
14. He J, Zhou X, Xu F, Shi Y, Okazaki T (2024) Seismic performance of self-centring connections with two energy dissipation stages for reusable modular steel buildings. Thin-Walled Structures 196:111442. https://doi.org/10.1016/j.tws.2023.111442.
15. Corfar D-A, Tsavdaridis KD (2023) A hybrid inter-module connection for steel modular building systems with SMA and high-damping rubber components. Engineering Structures 289:116281. https://doi.org/10.1016/j.engstruct.2023.116281.
16. Ahmadi H, Kingston J, Muhr AH (2008) Dynamic Properties of Filled Rubber - Part I: Simple Model, Experimental Data and Simulated Results. Rubber Chemistry and Technology 81:1–18. https://doi.org/10.5254/1.3548196.
17. Lindley PB, Gough J (2015) Engineering Design with Natural Rubber. 6th edn. Tun Abdul Razak Research Centre, Bertford.
18. Lacey AW, Chen W, Hao H (2022) Experimental methods for inter-module joints in modular building structures – A state-of-the-art review. Journal of Building Engineering 46:103792. https://doi.org/10.1016/j.jobe.2021.103792.
19. AISC (2022) Seismic Provisions for Structural Steel Buildings. American Institute of Steel Construction, Chicago.
20. SAC Joint Venture (2000) Recommended Seismic Design Criteria for New Steel Moment-Frame Buildings. Federal Emergency Management Agency, Washington, D.C.
21. BSI (2015) Eurocode 3: Design of steel structures - Part 1-1: General rules and rules for buildings. BSI, London.
22. Chen Z, Liu J, Yu Y, Zhou C, Yan R (2017) Experimental study of an innovative modular steel building connection. Journal of Constructional Steel Research 139:69–82. https://doi.org/10.1016/j.jcsr.2017.09.008.
23. Sanches R, Mercan O, Roberts B (2018) Experimental investigations of vertical post-tensioned connection for modular steel structures. Engineering Structures 175:776–89. https://doi.org/10.1016/j.engstruct.2018.08.049.
24. Zhai S-Y, Lyu Y-F, Cao K, Li G-Q, Wang W-Y, Chen C (2022) Experimental study on bolted-cover plate corner connections for column-supported modular steel buildings. Journal of Constructional Steel Research 189:107060. https://doi.org/10.1016/j.jcsr.2021.107060.
25. FEMA (2018) Seismic Performance Assessment of Buildings, Volume 1 – Methodology, 2nd edn. Federal Emergency Management Agency, Washington, D.C.